

## Measurements of baryon pair decays of $\chi_{cJ}$ mesons

M. Ablikim<sup>1</sup>, M. N. Achasov<sup>6</sup>, O. Albayrak<sup>3</sup>, D. J. Ambrose<sup>39</sup>, F. F. An<sup>1</sup>, Q. An<sup>40</sup>, J. Z. Bai<sup>1</sup>, Y. Ban<sup>26</sup>, J. Becker<sup>2</sup>, J. V. Bennett<sup>16</sup>, M. Bertani<sup>17A</sup>, J. M. Bian<sup>38</sup>, E. Boger<sup>19,a</sup>, O. Bondarenko<sup>20</sup>, I. Boyko<sup>19</sup>, R. A. Briere<sup>3</sup>, V. Bytev<sup>19</sup>, X. Cai<sup>1</sup>, O. Cakir<sup>34A</sup>, A. Calcaterra<sup>17A</sup>, G. F. Cao<sup>1</sup>, S. A. Cetin<sup>34B</sup>, J. F. Chang<sup>1</sup>, G. Chelkov<sup>19,a</sup>, G. Chen<sup>1</sup>, H. S. Chen<sup>1</sup>, J. C. Chen<sup>1</sup>, M. L. Chen<sup>1</sup>, S. J. Chen<sup>24</sup>, X. Chen<sup>26</sup>, Y. B. Chen<sup>1</sup>, H. P. Cheng<sup>14</sup>, Y. P. Chu<sup>1</sup>, D. Cronin-Hennessy<sup>38</sup>, H. L. Dai<sup>1</sup>, J. P. Dai<sup>1</sup>, D. Dedovich<sup>19</sup>, Z. Y. Deng<sup>1</sup>, A. Denig<sup>18</sup>, I. Denysenko<sup>19,b</sup>, M. Destefanis<sup>43A,43C</sup>, W. M. Ding<sup>28</sup>, Y. Ding<sup>22</sup>, L. Y. Dong<sup>1</sup>, M. Y. Dong<sup>1</sup>, S. X. Du<sup>46</sup>, J. Fang<sup>1</sup>, S. S. Fang<sup>1</sup>, L. Fava<sup>43B,43C</sup>, C. Q. Feng<sup>40</sup>, R. B. Ferroli<sup>17A</sup>, P. Friedel<sup>2</sup>, C. D. Fu<sup>1</sup>, Y. Gao<sup>33</sup>, C. Geng<sup>40</sup>, K. Goetzen<sup>7</sup>, W. X. Gong<sup>1</sup>, W. Gradl<sup>18</sup>, M. Greco<sup>43A,43C</sup>, M. H. Gu<sup>1</sup>, Y. T. Gu<sup>9</sup>, Y. H. Guan<sup>36</sup>, A. Q. Guo<sup>25</sup>, L. B. Guo<sup>23</sup>, T. Guo<sup>23</sup>, Y. P. Guo<sup>25</sup>, Y. L. Han<sup>1</sup>, F. A. Harris<sup>37</sup>, K. L. He<sup>1</sup>, M. He<sup>1</sup>, Z. Y. He<sup>25</sup>, T. Held<sup>2</sup>, Y. K. Heng<sup>1</sup>, Z. L. Hou<sup>1</sup>, C. Hu<sup>23</sup>, H. M. Hu<sup>1</sup>, J. F. Hu<sup>35</sup>, T. Hu<sup>1</sup>, G. M. Huang<sup>4</sup>, G. S. Huang<sup>40</sup>, J. S. Huang<sup>12</sup>, L. Huang<sup>1</sup>, X. T. Huang<sup>28</sup>, Y. Huang<sup>24</sup>, Y. P. Huang<sup>1</sup>, T. Hussain<sup>42</sup>, C. S. Ji<sup>40</sup>, Q. Ji<sup>1</sup>, Q. P. Ji<sup>25</sup>, X. B. Ji<sup>1</sup>, X. L. Ji<sup>1</sup>, L. L. Jiang<sup>1</sup>, X. S. Jiang<sup>1</sup>, J. B. Jiao<sup>28</sup>, Z. Jiao<sup>14</sup>, D. P. Jin<sup>1</sup>, S. Jin<sup>1</sup>, F. F. Jing<sup>33</sup>, N. Kalantar-Nayestanaki<sup>20</sup>, M. Kavatsyuk<sup>20</sup>, B. Kopf<sup>2</sup>, M. Kornicer<sup>37</sup>, W. Kuehn<sup>35</sup>, W. Lai<sup>1</sup>, J. S. Lange<sup>35</sup>, M. Leyhe<sup>2</sup>, C. H. Li<sup>1</sup>, Cheng Li<sup>40</sup>, Cui Li<sup>40</sup>, D. M. Li<sup>46</sup>, F. Li<sup>1</sup>, G. Li<sup>1</sup>, H. B. Li<sup>1</sup>, J. C. Li<sup>1</sup>, K. Li<sup>10</sup>, Lei Li<sup>1</sup>, Q. J. Li<sup>1</sup>, S. L. Li<sup>1</sup>, W. D. Li<sup>1</sup>, W. G. Li<sup>1</sup>, X. L. Li<sup>28</sup>, X. N. Li<sup>1</sup>, X. Q. Li<sup>25</sup>, X. R. Li<sup>27</sup>, Z. B. Li<sup>32</sup>, H. Liang<sup>40</sup>, Y. F. Liang<sup>30</sup>, Y. T. Liang<sup>35</sup>, G. R. Liao<sup>33</sup>, X. T. Liao<sup>1</sup>, D. Lin<sup>11</sup>, B. J. Liu<sup>1</sup>, C. L. Liu<sup>3</sup>, C. X. Liu<sup>1</sup>, F. H. Liu<sup>29</sup>, Fang Liu<sup>1</sup>, Feng Liu<sup>4</sup>, H. Liu<sup>1</sup>, H. B. Liu<sup>9</sup>, H. H. Liu<sup>13</sup>, H. M. Liu<sup>1</sup>, H. W. Liu<sup>1</sup>, J. P. Liu<sup>44</sup>, K. Liu<sup>33</sup>, K. Y. Liu<sup>22</sup>, Kai Liu<sup>36</sup>, P. L. Liu<sup>28</sup>, Q. Liu<sup>36</sup>, S. B. Liu<sup>40</sup>, X. Liu<sup>21</sup>, Y. B. Liu<sup>25</sup>, Z. A. Liu<sup>1</sup>, Zhiqiang Liu<sup>1</sup>, Zhiqing Liu<sup>1</sup>, H. Loehner<sup>20</sup>, G. R. Lu<sup>12</sup>, H. J. Lu<sup>14</sup>, J. G. Lu<sup>1</sup>, Q. W. Lu<sup>29</sup>, X. R. Lu<sup>36</sup>, Y. P. Lu<sup>1</sup>, C. L. Luo<sup>23</sup>, M. X. Luo<sup>45</sup>, T. Luo<sup>37</sup>, X. L. Luo<sup>1</sup>, M. Lv<sup>1</sup>, C. L. Ma<sup>36</sup>, F. C. Ma<sup>22</sup>, H. L. Ma<sup>1</sup>, Q. M. Ma<sup>1</sup>, S. Ma<sup>1</sup>, T. Ma<sup>1</sup>, X. Y. Ma<sup>1</sup>, F. E. Maas<sup>11</sup>, M. Maggiora<sup>43A,43C</sup>, Q. A. Malik<sup>42</sup>, Y. J. Mao<sup>26</sup>, Z. P. Mao<sup>1</sup>, J. G. Messchendorp<sup>20</sup>, J. Min<sup>1</sup>, T. J. Min<sup>1</sup>, R. E. Mitchell<sup>16</sup>, X. H. Mo<sup>1</sup>, C. Morales Morales<sup>11</sup>, N. Yu. Muchnoi<sup>6</sup>, H. Muramatsu<sup>39</sup>, Y. Nefedov<sup>19</sup>, C. Nicholson<sup>36</sup>, I. B. Nikolaev<sup>6</sup>, Z. Ning<sup>1</sup>, S. L. Olsen<sup>27</sup>, Q. Ouyang<sup>1</sup>, S. Pacetti<sup>17B</sup>, J. W. Park<sup>27</sup>, M. Pelizaeus<sup>2</sup>, H. P. Peng<sup>40</sup>, K. Peters<sup>7</sup>, J. L. Ping<sup>23</sup>, R. G. Ping<sup>1</sup>, R. Poling<sup>38</sup>, E. Prencipe<sup>18</sup>, M. Qi<sup>24</sup>, S. Qian<sup>1</sup>, C. F. Qiao<sup>36</sup>, L. Q. Qin<sup>28</sup>, X. S. Qin<sup>1</sup>, Y. Qin<sup>26</sup>, Z. H. Qin<sup>1</sup>, J. F. Qiu<sup>1</sup>, K. H. Rashid<sup>42</sup>, G. Rong<sup>1</sup>, X. D. Ruan<sup>9</sup>, A. Sarantsev<sup>19,c</sup>, B. D. Schaefer<sup>16</sup>, M. Shao<sup>40</sup>, C. P. Shen<sup>37,d</sup>, X. Y. Shen<sup>1</sup>, H. Y. Sheng<sup>1</sup>, M. R. Shepherd<sup>16</sup>, X. Y. Song<sup>1</sup>, S. Spataro<sup>43A,43C</sup>, B. Spruck<sup>35</sup>, D. H. Sun<sup>1</sup>, G. X. Sun<sup>1</sup>, J. F. Sun<sup>12</sup>, S. S. Sun<sup>1</sup>, Y. J. Sun<sup>40</sup>, Y. Z. Sun<sup>1</sup>, Z. J. Sun<sup>1</sup>, Z. T. Sun<sup>40</sup>, C. J. Tang<sup>30</sup>, X. Tang<sup>1</sup>, I. Tapan<sup>34C</sup>, E. H. Thorndike<sup>39</sup>, D. Toth<sup>38</sup>, M. Ullrich<sup>35</sup>, G. S. Varner<sup>37</sup>, B. Q. Wang<sup>26</sup>, D. Wang<sup>26</sup>, D. Y. Wang<sup>26</sup>, K. Wang<sup>1</sup>, L. L. Wang<sup>1</sup>, L. S. Wang<sup>1</sup>, M. Wang<sup>28</sup>, P. Wang<sup>1</sup>, P. L. Wang<sup>1</sup>, Q. J. Wang<sup>1</sup>, S. G. Wang<sup>26</sup>, X. F. Wang<sup>33</sup>, X. L. Wang<sup>40</sup>, Y. F. Wang<sup>1</sup>, Z. Wang<sup>1</sup>, Z. G. Wang<sup>1</sup>, Z. Y. Wang<sup>1</sup>, D. H. Wei<sup>8</sup>, J. B. Wei<sup>26</sup>, P. Weidenkaff<sup>18</sup>, Q. G. Wen<sup>40</sup>, S. P. Wen<sup>1</sup>, M. Werner<sup>35</sup>, U. Wiedner<sup>2</sup>, L. H. Wu<sup>1</sup>, N. Wu<sup>1</sup>, S. X. Wu<sup>40</sup>, W. Wu<sup>25</sup>, Z. Wu<sup>1</sup>, L. G. Xia<sup>33</sup>, Z. J. Xiao<sup>23</sup>, Y. G. Xie<sup>1</sup>, Q. L. Xiu<sup>1</sup>, G. F. Xu<sup>1</sup>, G. M. Xu<sup>26</sup>, Q. J. Xu<sup>10</sup>, Q. N. Xu<sup>36</sup>, X. P. Xu<sup>31</sup>, Z. R. Xu<sup>40</sup>, F. Xue<sup>4</sup>, Z. Xue<sup>1</sup>, L. Yan<sup>40</sup>, W. B. Yan<sup>40</sup>, Y. H. Yan<sup>15</sup>, H. X. Yang<sup>1</sup>, Y. Yang<sup>4</sup>, Y. X. Yang<sup>8</sup>, H. Ye<sup>1</sup>, M. Ye<sup>1</sup>, M. H. Ye<sup>5</sup>, B. X. Yu<sup>1</sup>, C. X. Yu<sup>25</sup>, H. W. Yu<sup>26</sup>, J. S. Yu<sup>21</sup>, S. P. Yu<sup>28</sup>, C. Z. Yuan<sup>1</sup>, Y. Yuan<sup>1</sup>, A. A. Zafar<sup>42</sup>, A. Zallo<sup>17A</sup>, Y. Zeng<sup>15</sup>, B. X. Zhang<sup>1</sup>, B. Y. Zhang<sup>1</sup>, C. Zhang<sup>24</sup>, C. C. Zhang<sup>1</sup>, D. H. Zhang<sup>1</sup>, H. H. Zhang<sup>32</sup>, H. Y. Zhang<sup>1</sup>,

J. Q. Zhang<sup>1</sup>, J. W. Zhang<sup>1</sup>, J. Y. Zhang<sup>1</sup>, J. Z. Zhang<sup>1</sup>, R. Zhang<sup>36</sup>, S. H. Zhang<sup>1</sup>,  
X. J. Zhang<sup>1</sup>, X. Y. Zhang<sup>28</sup>, Y. Zhang<sup>1</sup>, Y. H. Zhang<sup>1</sup>, Z. P. Zhang<sup>40</sup>, Z. Y. Zhang<sup>44</sup>,  
Zhenghao Zhang<sup>4</sup>, G. Zhao<sup>1</sup>, H. S. Zhao<sup>1</sup>, J. W. Zhao<sup>1</sup>, K. X. Zhao<sup>23</sup>, Lei Zhao<sup>40</sup>,  
Ling Zhao<sup>1</sup>, M. G. Zhao<sup>25</sup>, Q. Zhao<sup>1</sup>, Q. Z. Zhao<sup>9</sup>, S. J. Zhao<sup>46</sup>, T. C. Zhao<sup>1</sup>, Y. B. Zhao<sup>1</sup>,  
Z. G. Zhao<sup>40</sup>, A. Zhemchugov<sup>19,a</sup>, B. Zheng<sup>41</sup>, J. P. Zheng<sup>1</sup>, Y. H. Zheng<sup>36</sup>, B. Zhong<sup>23</sup>,  
Z. Zhong<sup>9</sup>, L. Zhou<sup>1</sup>, X. K. Zhou<sup>36</sup>, X. R. Zhou<sup>40</sup>, C. Zhu<sup>1</sup>, K. Zhu<sup>1</sup>, K. J. Zhu<sup>1</sup>, S. H. Zhu<sup>1</sup>,  
X. L. Zhu<sup>33</sup>, Y. C. Zhu<sup>40</sup>, Y. M. Zhu<sup>25</sup>, Y. S. Zhu<sup>1</sup>, Z. A. Zhu<sup>1</sup>, J. Zhuang<sup>1</sup>, B. S. Zou<sup>1</sup>, J. H. Zou<sup>1</sup>

(BESIII Collaboration)

- <sup>1</sup> *Institute of High Energy Physics, Beijing 100049, People's Republic of China*  
<sup>2</sup> *Bochum Ruhr-University, D-44780 Bochum, Germany*  
<sup>3</sup> *Carnegie Mellon University, Pittsburgh, Pennsylvania 15213, USA*  
<sup>4</sup> *Central China Normal University, Wuhan 430079, People's Republic of China*  
<sup>5</sup> *China Center of Advanced Science and Technology, Beijing 100190, People's Republic of China*  
<sup>6</sup> *G.I. Budker Institute of Nuclear Physics SB RAS (BINP), Novosibirsk 630090, Russia*  
<sup>7</sup> *GSI Helmholtzcentre for Heavy Ion Research GmbH, D-64291 Darmstadt, Germany*  
<sup>8</sup> *Guangxi Normal University, Guilin 541004, People's Republic of China*  
<sup>9</sup> *GuangXi University, Nanning 530004, People's Republic of China*  
<sup>10</sup> *Hangzhou Normal University, Hangzhou 310036, People's Republic of China*  
<sup>11</sup> *Helmholtz Institute Mainz, Johann-Joachim-Becher-Weg 45, D-55099 Mainz, Germany*  
<sup>12</sup> *Henan Normal University, Xinxiang 453007, People's Republic of China*  
<sup>13</sup> *Henan University of Science and Technology, Luoyang 471003, People's Republic of China*  
<sup>14</sup> *Huangshan College, Huangshan 245000, People's Republic of China*  
<sup>15</sup> *Hunan University, Changsha 410082, People's Republic of China*  
<sup>16</sup> *Indiana University, Bloomington, Indiana 47405, USA*  
<sup>17</sup> *(A)INFN Laboratori Nazionali di Frascati, I-00044, Frascati, Italy; (B)INFN and University of Perugia, I-06100, Perugia, Italy*  
<sup>18</sup> *Johannes Gutenberg University of Mainz, Johann-Joachim-Becher-Weg 45, D-55099 Mainz, Germany*  
<sup>19</sup> *Joint Institute for Nuclear Research, 141980 Dubna, Moscow region, Russia*  
<sup>20</sup> *KVI, University of Groningen, NL-9747 AA Groningen, The Netherlands*  
<sup>21</sup> *Lanzhou University, Lanzhou 730000, People's Republic of China*  
<sup>22</sup> *Liaoning University, Shenyang 110036, People's Republic of China*  
<sup>23</sup> *Nanjing Normal University, Nanjing 210023, People's Republic of China*  
<sup>24</sup> *Nanjing University, Nanjing 210093, People's Republic of China*  
<sup>25</sup> *Nankai University, Tianjin 300071, People's Republic of China*  
<sup>26</sup> *Peking University, Beijing 100871, People's Republic of China*  
<sup>27</sup> *Seoul National University, Seoul, 151-747 Korea*  
<sup>28</sup> *Shandong University, Jinan 250100, People's Republic of China*  
<sup>29</sup> *Shanxi University, Taiyuan 030006, People's Republic of China*  
<sup>30</sup> *Sichuan University, Chengdu 610064, People's Republic of China*  
<sup>31</sup> *Soochow University, Suzhou 215006, People's Republic of China*  
<sup>32</sup> *Sun Yat-Sen University, Guangzhou 510275, People's Republic of China*  
<sup>33</sup> *Tsinghua University, Beijing 100084, People's Republic of China*

<sup>34</sup> (A)Ankara University, Dogol Caddesi, 06100 Tandogan, Ankara, Turkey; (B)Dogus University, 34722 Istanbul, Turkey; (C)Uludag University, 16059 Bursa, Turkey

<sup>35</sup> Universitaet Giessen, D-35392 Giessen, Germany

<sup>36</sup> University of Chinese Academy of Sciences, Beijing 100049, People's Republic of China

<sup>37</sup> University of Hawaii, Honolulu, Hawaii 96822, USA

<sup>38</sup> University of Minnesota, Minneapolis, Minnesota 55455, USA

<sup>39</sup> University of Rochester, Rochester, New York 14627, USA

<sup>40</sup> University of Science and Technology of China, Hefei 230026, People's Republic of China

<sup>41</sup> University of South China, Hengyang 421001, People's Republic of China

<sup>42</sup> University of the Punjab, Lahore-54590, Pakistan

<sup>43</sup> (A)University of Turin, I-10125, Turin, Italy; (B)University of Eastern Piedmont, I-15121, Alessandria, Italy; (C)INFN, I-10125, Turin, Italy

<sup>44</sup> Wuhan University, Wuhan 430072, People's Republic of China

<sup>45</sup> Zhejiang University, Hangzhou 310027, People's Republic of China

<sup>46</sup> Zhengzhou University, Zhengzhou 450001, People's Republic of China

<sup>a</sup> Also at the Moscow Institute of Physics and Technology, Moscow 141700, Russia

<sup>b</sup> On leave from the Bogolyubov Institute for Theoretical Physics, Kiev 03680, Ukraine

<sup>c</sup> Also at the PNPI, Gatchina 188300, Russia

<sup>d</sup> Present address: Nagoya University, Nagoya 464-8601, Japan

## Abstract

Using  $106 \times 10^6$   $\psi'$  decays collected with the BESIII detector at the BEPCII, three decays of  $\chi_{cJ}$  ( $J = 0, 1, 2$ ) with baryon pairs ( $\Lambda\bar{\Lambda}$ ,  $\Sigma^0\bar{\Sigma}^0$ ,  $\Sigma^+\bar{\Sigma}^-$ ) in the final state have been studied. The branching fractions are measured to be  $\mathcal{B}(\chi_{c0,1,2} \rightarrow \Lambda\bar{\Lambda}) = (33.3 \pm 2.0 \pm 2.6) \times 10^{-5}$ ,  $(12.2 \pm 1.1 \pm 1.1) \times 10^{-5}$ ,  $(20.8 \pm 1.6 \pm 2.3) \times 10^{-5}$ ;  $\mathcal{B}(\chi_{c0,1,2} \rightarrow \Sigma^0\bar{\Sigma}^0) = (47.8 \pm 3.4 \pm 3.9) \times 10^{-5}$ ,  $(3.8 \pm 1.0 \pm 0.5) \times 10^{-5}$ ,  $(4.0 \pm 1.1 \pm 0.5) \times 10^{-5}$ ; and  $\mathcal{B}(\chi_{c0,1,2} \rightarrow \Sigma^+\bar{\Sigma}^-) = (45.4 \pm 4.2 \pm 3.0) \times 10^{-5}$ ,  $(5.4 \pm 1.5 \pm 0.5) \times 10^{-5}$ ,  $(4.9 \pm 1.9 \pm 0.7) \times 10^{-5}$ , where the first error is statistical and the second is systematic. Upper limits on the branching fractions for the decays of  $\chi_{c1,2} \rightarrow \Sigma^0\bar{\Sigma}^0$ ,  $\Sigma^+\bar{\Sigma}^-$ , are estimated to be  $\mathcal{B}(\chi_{c1} \rightarrow \Sigma^0\bar{\Sigma}^0) < 6.2 \times 10^{-5}$ ,  $\mathcal{B}(\chi_{c2} \rightarrow \Sigma^0\bar{\Sigma}^0) < 6.5 \times 10^{-5}$ ,  $\mathcal{B}(\chi_{c1} \rightarrow \Sigma^+\bar{\Sigma}^-) < 8.7 \times 10^{-5}$  and  $\mathcal{B}(\chi_{c2} \rightarrow \Sigma^+\bar{\Sigma}^-) < 8.8 \times 10^{-5}$  at the 90% confidence level.

PACS numbers: 12.38.Qk, 13.25.Gv, 14.20.Gk, 14.40.Gx

## 1 I. INTRODUCTION

2 In the standard quark model,  $\chi_{cJ}$  ( $J = 0, 1, 2$ ) mesons are  $c\bar{c}$  states in an  $L = 1$  configuration.  
3 Experimental studies on  $\chi_{cJ}$  decay properties are essential to test perturbative quantum chromody-  
4 namics (QCD) models and QCD-based calculations. The importance of the color octet mechanism  
5 for  $\chi_{cJ}$  decays has been pointed out for many years [1], and theoretical predictions of two-body  
6 exclusive decays have been made based on it. The predictions of the color octet mechanism theory  
7 for some  $\chi_{cJ}$  decays into baryon pairs ( $B\bar{B}$ ) disagree with measured values. For example, the  
8 branching fraction of  $\chi_{c0} \rightarrow \Lambda\bar{\Lambda}$  is predicted to be  $(93.5 \pm 20.5) \times 10^{-5}$  according to Ref. [2] and  
9  $(11.9 \sim 15.1) \times 10^{-5}$  according to Ref. [3], while the world average of experimental measure-  
10 ments is  $(33.0 \pm 4.0) \times 10^{-5}$  [4]. One finds that the theoretical prediction is either about two times  
11 larger, or several times smaller than the experimental measurement. Although some experimental  
12 results on  $\chi_{cJ}$  exclusive decays have been reported [5–7], many decay modes of  $\chi_{cJ} \rightarrow B\bar{B}$  have  
13 not been observed yet, such as  $\chi_{c1,2} \rightarrow \Sigma^0\bar{\Sigma}^0$ ,  $\Sigma^+\bar{\Sigma}^-$ , or measured with poor precision. For fur-  
14 ther testing of the color octet mechanism in the decays of the  $P$ -wave charmonia, measurements  
15 of other baryon pair decays of  $\chi_{cJ}$ , such as  $\chi_{cJ} \rightarrow \Lambda\bar{\Lambda}$ ,  $\Sigma^0\bar{\Sigma}^0$  and  $\Sigma^+\bar{\Sigma}^-$ , are desired.

16 In addition, measurements of  $\chi_{c0} \rightarrow B\bar{B}$  are helpful for further understanding the helicity  
17 selection rule [8], which prohibits  $\chi_{c0}$  decays into baryon-antibaryon pairs. However, the measured  
18 branching fractions for  $\chi_{c0} \rightarrow B\bar{B}$  do not vanish, for example  $\chi_{c0} \rightarrow p\bar{p}$  [4], which demonstrates  
19 a strong violation of the helicity selection rule in charmonium decays. It is necessary to measure  
20 the decays of  $\chi_{c0} \rightarrow B\bar{B}$  in other channels to provide additional tests of the helicity selection rule.

21 While  $\chi_{cJ}$  mesons are not produced directly in  $e^+e^-$  annihilations, the large branching fractions  
22 of  $\psi' \rightarrow \gamma\chi_{cJ}$  make  $e^+e^-$  collision at the  $\psi'$  peak a very clean environment for  $\chi_{cJ}$  investigation.  
23 In this paper, the results of two-body decays of  $\chi_{cJ} \rightarrow \Lambda\bar{\Lambda}$ ,  $\Sigma^0\bar{\Sigma}^0$  and  $\Sigma^+\bar{\Sigma}^-$  final states are  
24 presented. This analysis is based on  $106 \times 10^6$   $\psi'$  events [9] collected with BESIII at the BEPCII.  
25 A sample of  $44 \text{ pb}^{-1}$  of data taken at  $\sqrt{s} = 3.65 \text{ GeV}$  is used for continuum background study.

## 26 II. BESIII DETECTOR AND MONTE CARLO SIMULATION

27 BEPCII is a double-ring  $e^+e^-$  collider that has reached peak luminosity of about  $0.6 \times$   
28  $10^{33} \text{ cm}^{-2}\text{s}^{-1}$  at the peak energy of  $\psi(3770)$ . The cylindrical core of the BESIII detector con-  
29 sists of a helium-based main drift chamber (MDC), a plastic scintillator time-of-flight system,  
30 and a CsI(Tl) electromagnetic calorimeter (EMC), which are all enclosed in a superconducting  
31 solenoidal magnet providing a 1.0 T magnetic field. The solenoid is supported by an octagonal  
32 flux-return yoke with resistive plate counter muon identifier modules interleaved with steel. The  
33 acceptance for charged particles and photons is 93% over  $4\pi$  stereo angle, and the charged-particle  
34 momentum and photon energy resolutions at 1 GeV are 0.5% and 2.5%, respectively. The detector  
35 is described in more detail in Ref. [10].

36 The BESIII detector is modeled with a Monte Carlo (MC) simulation based on GEANT4 [11,  
37 12]. The  $\psi'$  resonance is produced with KKMC [13], while the subsequent decays are gener-  
38 ated with EVTGEN [14] according to the branching fractions provided by the Particle Data Group  
39 (PDG) [4], and the remaining unmeasured decay modes are generated with LUNDCHARM [15].

### 40 III. EVENT SELECTION

41 The investigated final states include  $\Lambda(\bar{\Lambda})$ ,  $p(\bar{p})$ , neutral  $\pi^0$  mesons and a radiative photon  
 42 from the decay  $\psi' \rightarrow \gamma\chi_{cJ}$ , where  $\Lambda(\bar{\Lambda})$  decays to  $\pi^-p(\pi^+\bar{p})$ , while  $\pi^0$  is reconstructed in the  
 43 decay to  $\pi^0 \rightarrow \gamma\gamma$ . Candidate events are required to satisfy the following selection criteria. A  
 44 charged track should have good quality in the track fitting and be within the angle coverage of  
 45 the MDC ( $|\cos\theta| < 0.92$ ). Photons are reconstructed from isolated showers in the EMC. The  
 46 energy deposited in the nearby TOF counter is included to improve the reconstruction efficiency  
 47 and energy resolution. Photon energies are required to be greater than 25 MeV in the EMC barrel  
 48 region ( $|\cos\theta| < 0.8$ ) and greater than 50 MeV in the EMC end cap ( $0.86 < |\cos\theta| < 0.92$ ).  
 49 The showers in the angular range between the barrel and the end cap are poorly reconstructed  
 50 and excluded from the analysis. Moreover, the EMC timing of the photon candidate must be in  
 51 coincidence with collision events,  $0 \leq t \leq 700$  ns, to suppress electronic noise and energy deposits  
 52 unrelated to the events.

#### 53 A. $\chi_{cJ} \rightarrow \Lambda\bar{\Lambda}$

54 Candidate events contain at least two positively charged tracks, two negatively charged tracks  
 55 and one photon. The  $\Lambda(\bar{\Lambda})$  candidates are reconstructed from pairs of oppositely charged tracks,  
 56 which are constrained to secondary vertices and have invariant masses closest to the nominal  $\Lambda$   
 57 mass. The  $\chi^2$  of the secondary vertex fit must be less than 500. The candidate photon and the  
 58  $\Lambda\bar{\Lambda}$  pair are subjected to a four constraint (4C) kinematic fit under the hypothesis of  $\psi' \rightarrow \gamma\Lambda\bar{\Lambda}$   
 59 to reduce background and improve the mass resolution. When additional photons are found in  
 60 an event, all possible combinations are iterated over, and the one with the best kinematic fit  $\chi_{4C}^2$   
 61 is kept. Furthermore,  $\chi_{4C}^2 < 50$  is required to suppress potential background from  $\psi' \rightarrow \Sigma^0\bar{\Sigma}^0$ .  
 62 The  $\chi_{4C}^2$  selection criterion is determined by optimizing the figure of merit (FOM),  $\text{FOM} = \frac{S}{\sqrt{S+B}}$ ,  
 63 where  $S$  is the number of signal events and  $B$  is the number of background events based on the  
 64 MC simulation. Figure 1(a) shows the comparison of  $\chi_{4C}^2$  between data and MC simulation,  
 65 which is normalized with the number of events satisfying the  $\chi^2$  requirement. Figure 1(b) shows  
 66 the scatter plots of  $M_{p\pi^-}$  versus  $M_{\bar{p}\pi^+}$  from the data. Clear  $\Lambda\bar{\Lambda}$  signals can be seen. The square  
 67 around the  $\Lambda$  nominal mass with a width of  $20 \text{ MeV}/c^2$  is taken as the signal region, which is also  
 68 determined by maximizing the FOM. From events with two or more photons, additional selection  
 69 criteria are applied to suppress backgrounds from  $\Sigma^0\bar{\Sigma}^0$  decays. The  $\psi' \rightarrow \Sigma^0\bar{\Sigma}^0$  candidates  
 70 are selected by minimizing  $\sqrt{(M_{\gamma\Lambda} - M_{\Sigma^0})^2 + (M_{\gamma\bar{\Lambda}} - M_{\bar{\Sigma}^0})^2}$  from all combinations. However,  
 71 some backgrounds remain in the signal region from  $\psi' \rightarrow \Sigma^0\bar{\Sigma}^0$  events in which one photon from  
 72 the  $\Sigma^0$  decays is not reconstructed. To remove these, events falling into  $|M_{\gamma\Lambda} - M_{\Sigma^0}| < 6 \text{ MeV}/c^2$   
 73 and  $|M_{\gamma\bar{\Lambda}} - M_{\bar{\Sigma}^0}| < 6 \text{ MeV}/c^2$  have been discarded.

#### 74 B. $\chi_{cJ} \rightarrow \Sigma^0\bar{\Sigma}^0$

75 Candidate events have at least two positively charged tracks, two negatively charged tracks and  
 76 three photons. The charged track selection and  $\Lambda(\bar{\Lambda})$  reconstruction are the same as described  
 77 above for the  $\chi_{cJ} \rightarrow \Lambda\bar{\Lambda}$  decay. The mass window of  $\Lambda(\bar{\Lambda})$  is optimized to be  $|M_{p\pi} - M_{\Lambda}| <$   
 78  $7 \text{ MeV}/c^2$ . The candidate photons and the  $\Lambda\bar{\Lambda}$  pair are subjected to a 4C kinematic fit under

79 the hypothesis of  $\psi' \rightarrow \gamma\gamma\gamma\Lambda\bar{\Lambda}$  to reduce background and improve the mass resolution. When  
80 additional photons are found in an event, all possible combinations are looped over, the one with  
81 the smallest  $\chi_{4C}^2$  is kept, and  $\chi_{4C}^2 < 35$  is required to suppress the dominant background from  
82  $\psi' \rightarrow \Sigma^0\bar{\Sigma}^0$ . Figure 1(c) shows the comparison of  $\chi_{4C}^2$  between data and MC simulation, which  
83 is normalized with the number of events satisfying the  $\chi^2$  requirement. The  $\Sigma^0\bar{\Sigma}^0$  candidates are  
84 chosen by minimizing  $\sqrt{(M_{\gamma\Lambda} - M_{\Sigma^0})^2 + (M_{\gamma\bar{\Lambda}} - M_{\bar{\Sigma}^0})^2}$ . Figure 1(d) shows the scatter plot of  
85  $M_{\gamma\Lambda}$  versus  $M_{\gamma\bar{\Lambda}}$  from the data. Clear  $\Sigma^0\bar{\Sigma}^0$  signals can be seen. The square around the  $\Sigma^0$  nominal  
86 mass with a width of  $32 \text{ MeV}/c^2$  represents the signal region.

### 87 C. $\chi_{cJ} \rightarrow \Sigma^+\bar{\Sigma}^-$

88 Candidate events contain at least one positively charged, one negatively charged tracks and  
89 five photons. We impose a 4C kinematic fit to the selected tracks and photons under the  
90  $\psi' \rightarrow 5\gamma p\bar{p}$  hypothesis and keep the one with the smallest  $\chi_{4C}^2$ , and  $\chi_{4C}^2 < 50$  is required to  
91 suppress the dominant background from  $\psi' \rightarrow \Sigma^+\bar{\Sigma}^-$ . Figure 1(e) shows the comparison of  
92  $\chi_{4C}^2$  between data and MC simulation, which is normalized with the number of events satisfy-  
93 ing the  $\chi^2$  requirement. The  $\pi^0$  candidates are reconstructed by selecting the combination  
94 which minimizes  $\sqrt{(M_{\gamma\gamma}^{(1)} - M_{\pi^0})^2 + (M_{\gamma\gamma}^{(2)} - M_{\pi^0})^2}$ . The  $\Sigma^+\bar{\Sigma}^-$  pair is selected by minimizing  
95  $\sqrt{(M_{p\pi^0} - M_{\Sigma^+})^2 + (M_{\bar{p}\pi^0} - M_{\bar{\Sigma}^-})^2}$ . Figure 1(f) shows the scatter plot of  $M_{p\pi^0}$  versus  $M_{\bar{p}\pi^0}$   
96 from the data. Clear  $\Sigma^+\bar{\Sigma}^-$  signals can be seen. The square of  $1.17 \text{ GeV}/c^2 < M_{p\pi^0} < 1.20$   
97  $\text{GeV}/c^2$  and  $1.17 \text{ GeV}/c^2 < M_{\bar{p}\pi^0} < 1.20 \text{ GeV}/c^2$  denotes the signal region.

## 99 IV. BACKGROUND STUDY

### 100 A. Continuum backgrounds

101 The events collected at  $E_{\text{cm}} = 3.65 \text{ GeV}$ , whose integrated luminosity is more than 1/4 of  $\psi'$   
102 samples, are analyzed to estimate the contribution from the continuum process. No events are  
103 survived in the  $\Lambda\bar{\Lambda}$ ,  $\Sigma^0\bar{\Sigma}^0$  and  $\Sigma^+\bar{\Sigma}^-$  signal regions. Therefore, backgrounds from the continuum  
104 are neglected.

### 105 B. Dominant backgrounds in $\Lambda\bar{\Lambda}$ , $\Sigma^0\bar{\Sigma}^0$ and $\Sigma^+\bar{\Sigma}^-$ final states

106 By using  $106 \times 10^6$  inclusive MC events, we find that the dominant background for  $\chi_{cJ} \rightarrow \Lambda\bar{\Lambda}$   
107 comes from the decay  $\psi' \rightarrow \Sigma^0\bar{\Sigma}^0$  in which one photon is missing. The non- $\Lambda\bar{\Lambda}$  background from  
108 the decay  $\chi_{cJ} \rightarrow \pi^+\pi^-p\bar{p}$  is negligibly small due to the low efficiency near the mass threshold.  
109 For  $\chi_{cJ} \rightarrow \Sigma^0\bar{\Sigma}^0$ , the dominant background is also found to arise from  $\psi' \rightarrow \Sigma^0\bar{\Sigma}^0$ . But this  
110 background mainly distributes around the  $\psi'$  mass region in the  $\Sigma^0\bar{\Sigma}^0$  invariant mass. In addition,  
111 a few background events come from  $\psi' \rightarrow \pi^0\pi^0 J/\psi$  and  $\psi' \rightarrow \Xi^0\bar{\Xi}^0$ . For  $\chi_{cJ} \rightarrow \Sigma^+\bar{\Sigma}^-$ , the  
112 backgrounds are small; they are from the decay  $\psi' \rightarrow \Sigma^+\bar{\Sigma}^-$ ,  $\psi' \rightarrow \pi^0\pi^0 J/\psi$  and  $J/\psi \rightarrow p\bar{p}$   
113 (or  $\gamma p\bar{p}$ ). The contributions of all backgrounds mentioned above are estimated by MC simulation  
114 according to their branching fractions.

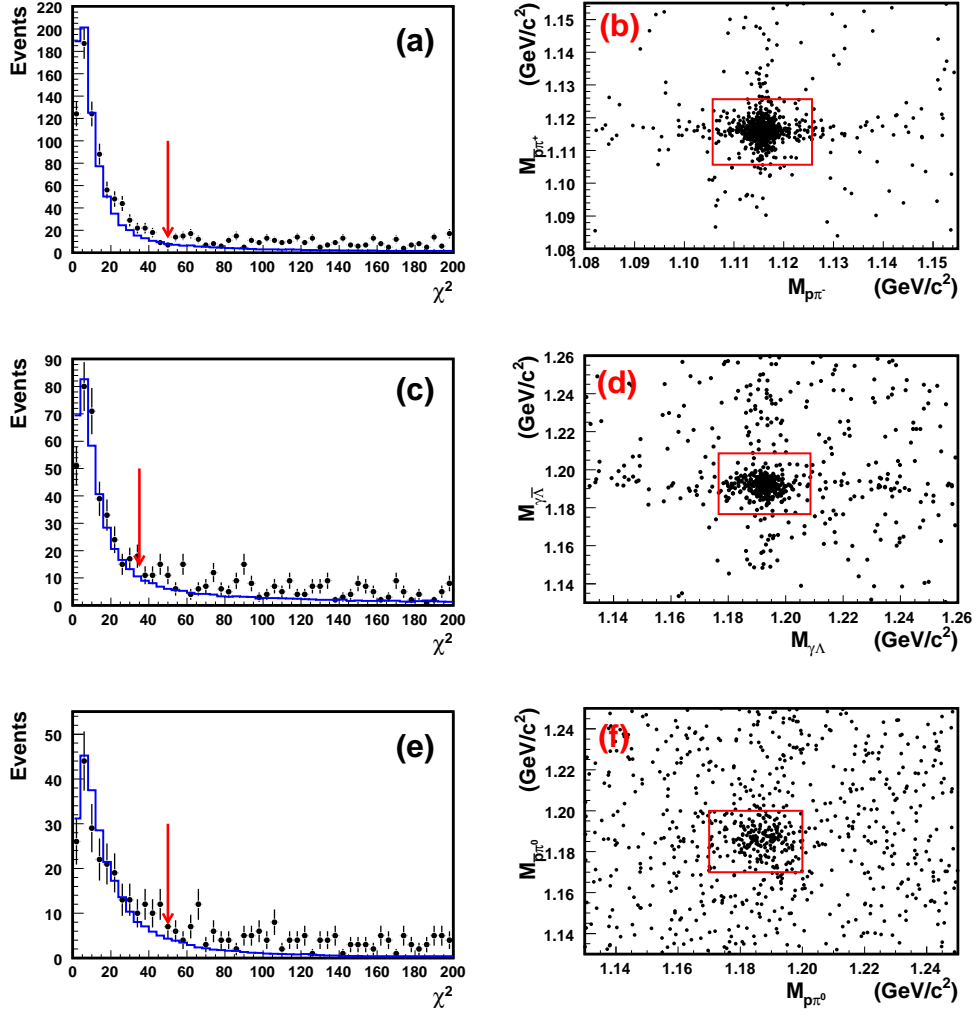


FIG. 1. (a) The  $\chi_{4C}^2$  distribution and (b)  $M_{p\pi^-}$  versus  $M_{\bar{p}\pi^+}$  (data) for the  $\psi' \rightarrow \gamma\chi_{cJ}, \chi_{cJ} \rightarrow \Lambda\bar{\Lambda}$  candidates; (c) the  $\chi_{4C}^2$  distribution and (d)  $M_{\gamma\Lambda}$  versus  $M_{\gamma\bar{\Lambda}}$  (data) for the  $\psi' \rightarrow \gamma\chi_{cJ}, \chi_{cJ} \rightarrow \Sigma^0\bar{\Sigma}^0$  candidates; (e) the  $\chi_{4C}^2$  distribution and (f)  $M_{p\pi^0}$  versus  $M_{\bar{p}\pi^0}$  (data) for the  $\psi' \rightarrow \gamma\chi_{cJ}, \chi_{cJ} \rightarrow \Sigma^+\bar{\Sigma}^-$  candidates.

## 115 V. FIT TO THE SIGNAL OF $\chi_{cJ}$

116 The invariant mass of the baryon pairs  $M_{B\bar{B}}$  for all selected events are shown in Figs. 2(a)–  
 117 (b) for  $\chi_{cJ} \rightarrow \Lambda\bar{\Lambda}$ ,  $\Sigma^0\bar{\Sigma}^0$  and  $\Sigma^+\bar{\Sigma}^-$ , respectively. Clear  $\chi_{c0,1,2}$  signals can be seen in  $\Lambda\bar{\Lambda}$  final  
 118 state, and a clear  $\chi_{c0}$  signal is seen in both  $\Sigma^0\bar{\Sigma}^0$  and  $\Sigma^+\bar{\Sigma}^-$  final states, while the  $\chi_{c1,2}$  signals  
 119 are not significant in  $\Sigma^0\bar{\Sigma}^0$  and  $\Sigma^+\bar{\Sigma}^-$  final states. We fit the invariant mass spectra of baryon  
 120 pairs,  $M_{B\bar{B}}$ , to extract the numbers of  $\chi_{cJ}$  signal events, where the signals are represented by  
 121 Breit-Wigner functions convolved with a Crystal Ball function to account for the detector resolu-  
 122 tion, a second-order Chebychev polynomial is used to describe non-peaking backgrounds, and the  
 123 dominant background events, estimated by MC simulation, have been directly subtracted from the  
 124 data. The widths of the Breit-Wigner functions were fixed according to the known values [4], the  
 125 parameters of the Crystal Ball function are fixed based on MC simulation, and these parameters

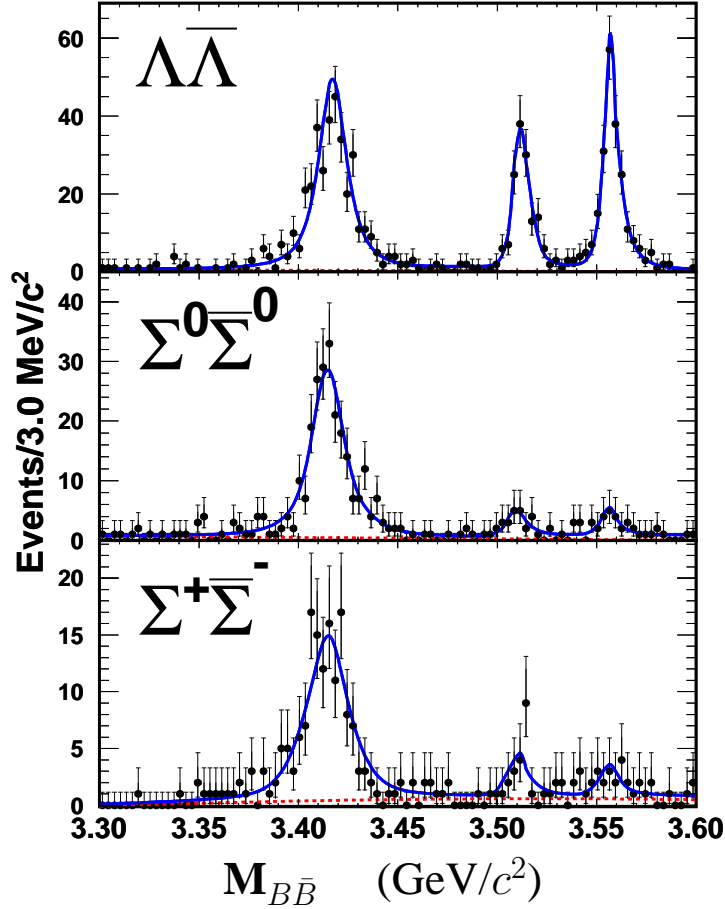


FIG. 2. The fit to the invariant mass  $M_{B\bar{B}}$ . The dots with error bars are for data. The solid line is the fit results. Dashed-line is other background. The parameters of signal function are fixed to those obtained from MC simulation.

126 are varied by  $\pm \sigma$  for the determination of systematic uncertainties. To determine the goodness of  
 127 fit, we bin the data so that the number of events in each bin is at least ten. The calculated  $\chi^2/\text{d.o.f}$  is  
 128 1.03, 1.53 and 1.71 for the  $\Lambda\bar{\Lambda}$ ,  $\Sigma^0\bar{\Sigma}^0$  and  $\Sigma^+\bar{\Sigma}^-$  final states, respectively. The numbers of  $\chi_{c0,1,2}$   
 129 signal events from the fits are listed in Table I. For the decay  $\chi_{c1,2} \rightarrow \Sigma^0\bar{\Sigma}^0$ ,  $\Sigma^+\bar{\Sigma}^-$ , the upper limits  
 130 of the branching fractions at the 90% C.L. are also determined with a Bayesian method [16]. The  
 131 statistical significances of the signals are calculated as  $\sqrt{-2\Delta \ln \mathcal{L}}$ , where  $\Delta \ln \mathcal{L}$  is the difference  
 132 between the logarithmic maximum likelihood values of the fit with and without the corresponding  
 133 signal function. They are  $4.3\sigma$  and  $4.6\sigma$  for  $\chi_{c1,2} \rightarrow \Sigma^0\bar{\Sigma}^0$ , and  $4.4\sigma$  and  $3.0\sigma$  for  $\chi_{c1,2} \rightarrow \Sigma^+\bar{\Sigma}^-$ ,  
 134 respectively. The signal efficiencies determined from MC simulation are also listed in Table I,  
 135 where the proper angular distributions for photons emitted in  $\psi' \rightarrow \gamma\chi_{cJ}$  are used [17]. The decay  
 136 of  $\chi_{cJ} \rightarrow B\bar{B}$  and the decay of baryons are generated with a phase space model.



TABLE I. Efficiencies ( $\epsilon$  in %) obtained from MC simulation, and the signal yields  $N^{obs}$  determined from fit.

Mode	$\chi_{c0}$		$\chi_{c1}$		$\chi_{c2}$	
	$N^{obs}$	$\epsilon$	$N^{obs}$	$\epsilon$	$N^{obs}$	$\epsilon$
$\Lambda\bar{\Lambda}$	$368.9 \pm 22.1$	$26.6 \pm 0.2$	$135.6 \pm 12.6$	$27.9 \pm 0.2$	$207.1 \pm 15.7$	$26.3 \pm 0.2$
$\Sigma^0\bar{\Sigma}^0$	$242.8 \pm 17.1$	$12.2 \pm 0.1$	$20.0 \pm 5.3$	$13.2 \pm 0.1$	$18.9 \pm 5.3$	$12.7 \pm 0.1$
$\Sigma^+\bar{\Sigma}^-$	$147.8 \pm 13.8$	$12.3 \pm 0.1$	$18.0 \pm 5.4$	$13.1 \pm 0.1$	$14.5 \pm 5.6$	$12.3 \pm 0.1$

## 139 VI. SYSTEMATIC ERROR

140 The systematic errors mainly originate from the uncertainties of the tracking efficiency,  $\Lambda(\bar{\Lambda})$   
 141 reconstruction efficiency, the photon efficiency, 4C kinematic fit, the branching fractions of the  
 142 intermediate states, fit range, the angular distribution of  $\chi_{c1,2} \rightarrow B\bar{B}$ , background shape, signal  
 143 line shape, MC resolution and the total number of  $\psi'$  events.

- 144 1. The decay  $\psi' \rightarrow \Lambda\bar{\Lambda}$  with  $\Lambda \rightarrow p\pi^-$  and  $\Lambda \rightarrow \bar{p}\pi^-$  is employed to study the  $\Lambda(\bar{\Lambda})$  recon-  
 145 struction efficiency. The selection criteria of charged tracks are the same as before except  
 146 we use particle identification information to suppress background. Candidate events have  
 147 at least one positively charged and one negatively charged tracks, which are required to be  
 148 identified as a  $\pi^+(\pi^-)$  track and an  $\bar{p}(p)$  track, respectively. Also, the invariant mass of  
 149  $\pi^+\bar{p}(\pi^-p)$  must be within 10 MeV/ $c^2$  of the nominal  $\bar{\Lambda}$  mass. Furthermore, the momentum  
 150 of  $\bar{\Lambda}(\Lambda)$  candidates is required to be within 20 MeV/ $c$  of its nominal value in two-body de-  
 151 cay of  $\psi' \rightarrow \Lambda\bar{\Lambda}$ . The number of  $\Lambda$  signal events,  $N_{\Lambda}^0$ , is extracted by fitting the recoiling  
 152 mass spectrum of  $\bar{\Lambda}$ ,  $M_{recoil}^{\bar{\Lambda}}$ . Then two additional opposite charged tracks, a  $\pi^-(\pi^+)$  and a  
 153  $p(\bar{p})$ , are required to reconstruct  $\Lambda$  and are constrained to the secondary vertex. The number  
 154 of  $\Lambda$  signal events,  $N_{\Lambda}^1$ , is extracted by fitting  $M_{recoil}^{\Lambda}$  after requiring a  $\Lambda$  secondary vertex  
 155 constraint. The  $\Lambda(\bar{\Lambda})$  reconstruction efficiency is determined as  $\epsilon_{\Lambda} = \frac{N_{\Lambda}^1}{N_{\Lambda}^0}$ . The difference of  
 156 the efficiencies between data and MC simulation is found to be 2.0% for a  $\Lambda$  and 5.0% for a  
 157  $\bar{\Lambda}$ , which are taken as the systematic error due to  $\Lambda(\bar{\Lambda})$  reconstruction efficiency.
- 158 2. Since the decay length for  $\Sigma^+(\bar{\Sigma}^-)$  is small, the decay  $J/\psi \rightarrow \pi^+\pi^-p\bar{p}$  is used to study the  
 159 MDC tracking efficiency for the proton and antiproton of the  $\Sigma^+\bar{\Sigma}^-$  final state. It is found  
 160 that the efficiency for MC simulated events agrees with that determined from data within  
 161 1.0% for each charged track. Hence, 2.0% is taken as the systematic error for the proton and  
 162 antiproton of the  $\Sigma^+\bar{\Sigma}^-$  final state.
- 163 3. The uncertainty due to photon detection efficiency is 1% per photon, which is determined  
 164 from the decay  $J/\psi \rightarrow \rho\pi$  [18].
- 165 4. Five decays,  $J/\psi \rightarrow \Lambda\bar{\Lambda}$ ,  $J/\psi \rightarrow \Sigma^0\bar{\Sigma}^0$ ,  $J/\psi \rightarrow \Xi^0\bar{\Xi}^0$ ,  $\psi' \rightarrow \pi^0\pi^0 J/\psi$  ( $J/\psi \rightarrow p\bar{p}$ )  
 166 and  $\psi' \rightarrow \pi^0\pi^0 J/\psi$  ( $J/\psi \rightarrow p\bar{p}\pi^0$ ), are used to study the efficiencies of the 4C kinematic  
 167 fits. The signal events are selected from data and inclusive MC events without the 4C fit  
 168 information. The remaining background is found to be negligible according to the studies  
 169 of the inclusive MC events. The efficiency of the 4C kinematic fit is defined as  $\frac{N_1}{N_0}$ , where  
 170  $N_0$  is the the number of signal events, and  $N_1$  is the number of events survived. For the  
 171  $\chi_{cJ} \rightarrow \Lambda\bar{\Lambda}$ , where the final state is  $\psi' \rightarrow \gamma\Lambda\bar{\Lambda}$ , two decays,  $J/\psi \rightarrow \Lambda\bar{\Lambda}$ , and  $J/\psi \rightarrow$

172  $\Sigma^0\bar{\Sigma}^0$ , are used to investigate the systematic error due to the 4C kinematic fit. The final  
 173 states of these two control samples contain one photon less or more than the signal channel.  
 174 Conservatively, the larger difference observed in the two control samples, 2.4%, is taken as  
 175 the systematic error. Similarly, the larger difference in  $J/\psi \rightarrow \Sigma^0\bar{\Sigma}^0$  and  $J/\psi \rightarrow \Xi^0\bar{\Xi}^0$ ,  
 176 2.9%, is taken as the systematic error of the  $\chi_{cJ} \rightarrow \Sigma^0\bar{\Sigma}^0$  channel, and the larger difference  
 177 in  $\psi' \rightarrow \pi^0\pi^0 J/\psi$  ( $J/\psi \rightarrow p\bar{p}$ ) and  $\psi' \rightarrow \pi^0\pi^0 J/\psi$  ( $J/\psi \rightarrow p\bar{p}\pi^0$ ), 1.3%, is taken as the  
 178 error of  $\chi_{cJ} \rightarrow \Sigma^+\bar{\Sigma}^-$ .

179 5. When changing mass ranges in fitting  $M_{B\bar{B}}$  signals to 3.30–3.62 GeV/ $c^2$  or to 3.25–3.62  
 180 GeV/ $c^2$ , the fitted numbers of  $\chi_{c0,1,2}$  have some changes for data and MC simulation. Tak-  
 181 ing the  $\Lambda\bar{\Lambda}$  channel as an example, the results in the range of 3.30 GeV/ $c^2$  to 3.60 GeV/ $c^2$   
 182 are taken as central values, when the fit range is changed to 3.32–3.60 GeV/ $c^2$ , the changes  
 183 relative to central values are found to be 2.7%, 3.6% and 2.2% for the  $\chi_{c0,1,2}$  decays, re-  
 184 spectively, while in the range 3.25–3.62 GeV/ $c^2$ , the changes are found to be 2.2%, 0.9%  
 185 and 4.3%. Conservatively, we take the larger ones, 2.7%, 3.6% and 4.3%, as the systematic  
 186 errors for the  $\Lambda\bar{\Lambda}$  final state. With the same method, the systematic errors for the other two  
 187 channels are determined to be 1.4%, 6.7% and 4.3% for the  $\Sigma^0\bar{\Sigma}^0$  final state and 1.4%, 3.0%  
 188 and 7.2% for the  $\Sigma^+\bar{\Sigma}^-$  final state.

189 6. In the fits to the  $M_{B\bar{B}}$  invariant mass, the signals are described by a parameterized shape  
 190 obtained from MC simulation in which the widths of  $\chi_{cJ}$  are fixed since we only observe a  
 191 small number of signal events in  $\chi_{c1,2} \rightarrow \Sigma^0\bar{\Sigma}^0$  and  $\Sigma^+\bar{\Sigma}^-$ . When changing the parameters  
 192 of  $\chi_{cJ}$  widths in this MC simulation by  $\pm \sigma$ , it is found that the difference of the numbers  
 193 of fitted  $\chi_{c1,2}$  events between data and MC is 1.2%, 0.0% and 0.0% for the  $\Lambda\bar{\Lambda}$  final state;  
 194 1.9%, 0.0% and 3.7% for the  $\Sigma^0\bar{\Sigma}^0$  final state and 1.0%, 0.5% and 2.0% for the  $\Sigma^+\bar{\Sigma}^-$  final  
 195 state. Hence, we take the difference as the systematic error due to the  $\chi_{cJ}$  widths.

196 7. The partial width for an E1/M1 radiative transition is proportional to the cube of the radiative  
 197 photon energy ( $E_\gamma^3$ ), which leads to a diverging tail in the lower mass region. Two damping  
 198 factors have been proposed by the KEDR [19] and the CLEO [20] Collaborations and have  
 199 been included to describe the signal line shape. Differences in the signal yields with respect  
 200 to the fit not taking into account this damping factor are observed, and the greater differences  
 201 are 0.7%, 2.1% and 2.7% for the  $\Lambda\bar{\Lambda}$  final state; 1.4%, 1.0% and 2.2% for the  $\Sigma^0\bar{\Sigma}^0$  final  
 202 state; 0.0%, 2.7% and 5.5% for the  $\Sigma^+\bar{\Sigma}^-$  final state, which are taken as the systematic error  
 203 associated with the signal line shape.

204 8. From the decay  $J/\psi \rightarrow \Lambda\bar{\Lambda}$ , it is found that the average resolution is  $7.90 \pm 0.09$  MeV/ $c^2$   
 205 for the data and  $7.08 \pm 0.04$  MeV/ $c^2$  for MC. Differences in fitting the  $\chi_{cJ}$  signal with and  
 206 without fixing the MC parameters are found to be 1.5%, 0.5% and 2.4% for the  $\Lambda\bar{\Lambda}$  final  
 207 states, which are taken as the systematic error of the resolution. However, from the decays  
 208  $J/\psi \rightarrow \Sigma^0\bar{\Sigma}^0$  and  $J/\psi \rightarrow \Sigma^+\bar{\Sigma}^-$ , one can find that the resolutions between data and MC  
 209 are consistent. Therefore, the systematic errors of the resolution for the  $\Sigma^0\bar{\Sigma}^0$  and  $\Sigma^+\bar{\Sigma}^-$   
 210 final state are neglected.

211 9. To estimate the uncertainty of the angular distribution, we use another model in which the  
 212 angular distribution of  $\chi_{c1,2} \rightarrow B\bar{B}$  is taken into account according to the helicity ampli-  
 213 tude [21]. When the two independent helicity amplitudes,  $B_{\frac{1}{2},-\frac{1}{2}}$  and  $B_{-\frac{1}{2},\frac{1}{2}}$ , are set to be  
 214 1.0, the efficiencies are found to be  $(28.8 \pm 0.2)\%$  and  $(27.9 \pm 0.2)\%$  for the  $\chi_{c1,2} \rightarrow \Lambda\bar{\Lambda}$

215  
216  
217  
218

final state, respectively. The differences from phase space are 3.2% and 6.0%. Similar comparisons are also done for the  $\Sigma^0\bar{\Sigma}^0$  and  $\Sigma^+\bar{\Sigma}^-$  final states, and the differences are smaller. Conservatively, we take the difference of the  $\Lambda\bar{\Lambda}$  final state as the systematic error of the angular distribution for all  $B\bar{B}$  final states.

219  
220  
221  
222

10. In Fig. 2, the combinatorial background curves are fitted with a second-order Chebychev polynomial. The background function is changed to first- and third-order polynomials, and the largest difference is taken as the systematic error due to the uncertainty in the description of the background shape.

223  
224

11. The total number of  $\psi'$  events are obtained by studying inclusive hadronic  $\psi'$  decays with an uncertainty of 0.81% [9].

225  
226

Table II lists all systematic error contributions, and the total systematic error is obtained by adding the individual contributions in quadrature.

TABLE II. Systematic errors in the branching fraction measurements (%)

Source	$\chi_{cJ} \rightarrow \Lambda\bar{\Lambda}$			$\chi_{cJ} \rightarrow \Sigma^0\bar{\Sigma}^0$			$\chi_{cJ} \rightarrow \Sigma^+\bar{\Sigma}^-$		
	$\chi_{c0}$	$\chi_{c1}$	$\chi_{c2}$	$\chi_{c0}$	$\chi_{c1}$	$\chi_{c2}$	$\chi_{c0}$	$\chi_{c1}$	$\chi_{c2}$
The total number of $\psi'$	0.81	0.81	0.81	0.81	0.81	0.81	0.81	0.81	0.81
MDC tracking ( $p, \bar{p}$ )	–	–	–	–	–	–	2.0	2.0	2.0
Photon efficiency	1.0	1.0	1.0	3.0	3.0	3.0	5.0	5.0	5.0
$\Lambda$ reconstruction	2.0	2.0	2.0	2.0	2.0	2.0	–	–	–
$\bar{\Lambda}$ reconstruction	5.0	5.0	5.0	5.0	5.0	5.0	–	–	–
Kinematic fit	2.4	2.4	2.4	2.9	2.9	2.9	1.3	1.3	1.3
Fitting range	2.7	3.6	4.3	1.4	6.7	4.3	1.4	3.0	7.2
$\chi_{cJ}$ width	1.2	0.0	0.0	1.9	0.0	3.7	1.0	0.5	2.0
Angular distribution	0.0	3.2	6.0	0.0	3.2	6.0	0.0	3.2	6.0
Background shape	0.5	1.3	1.3	1.7	7.8	6.0	1.8	2.5	3.0
Signal line shape	0.7	2.1	2.7	1.4	1.0	2.2	0.0	2.7	5.5
MC resolution	1.5	0.5	2.4	0.0	0.0	0.0	0.0	0.0	0.0
$\mathcal{B}(\psi' \rightarrow \gamma\chi_{cJ})$	3.2	4.3	4.0	3.2	4.3	4.0	3.2	4.3	4.0
$\mathcal{B}(\Sigma \rightarrow p\pi)$	–	–	–	–	–	–	0.82	0.82	0.82
$\mathcal{B}(\Lambda \rightarrow p\pi)$	1.1	1.1	1.1	1.1	1.1	1.1	–	–	–
Total systematic error	7.7	9.3	11.1	8.3	13.6	13.2	7.0	9.1	13.4

227  
228

## 229 VII. RESULTS

230

The branching fraction of  $\chi_{cJ} \rightarrow B\bar{B}$  is determined by

$$\mathcal{B}(\chi_{cJ} \rightarrow B\bar{B}) = \frac{N^{obs}[\chi_{cJ}]}{N_{\psi'} \cdot \epsilon \cdot \prod_i \mathcal{B}_i},$$

231 and if the signal is not significant, the corresponding upper limit of branching fraction is set with

$$\mathcal{B}(\chi_{cJ} \rightarrow B\bar{B}) < \frac{N_{UL}^{obs}[\chi_{cJ}]}{N_{\psi'} \cdot \epsilon \cdot \prod_i \mathcal{B}_i \cdot (1.0 - \sigma_{sys})},$$

232 where,  $N^{obs}$  is the number of observed signal events and  $N_{UL}^{obs}$  is the upper limit of the number of  
 233 events,  $\epsilon$  is the detection efficiency shown in Table I,  $\sigma_{sys}$  is the relative the systematic error,  $N_{\psi'}$   
 234 is the total number of  $\psi'$  events [9], and  $\prod_i \mathcal{B}_i$  is the product of the branching fractions taken from  
 235 the world average [4] for the  $\psi' \rightarrow \gamma\chi_{cJ}$  and the other decays that are involved. With the numbers  
 236 listed in Table I and the branching fractions for the relevant baryon decays, the branching fractions  
 237 or the upper limits at the 90% C.L. for  $\chi_{cJ}$  decays are determined, as listed in Table III.

TABLE III. Branching fractions (or their upper limits) of  $\chi_{cJ} \rightarrow \Lambda\bar{\Lambda}$ ,  $\Sigma^0\bar{\Sigma}^0$  and  $\Sigma^+\bar{\Sigma}^-$  (in units of  $10^{-5}$ ). The first error is statistical and the second is systematic.

Mode		$\chi_{c0}$	$\chi_{c1}$	$\chi_{c2}$
$\Lambda\bar{\Lambda}$	This work	$33.3 \pm 2.0 \pm 2.6$	$12.2 \pm 1.1 \pm 1.1$	$20.8 \pm 1.6 \pm 2.3$
	PDG	$33.0 \pm 4.0$	$11.8 \pm 1.9$	$18.6 \pm 2.7$
	CLEO	$33.8 \pm 3.6 \pm 2.2 \pm 1.7$	$11.6 \pm 1.8 \pm 0.7 \pm 0.7$	$17.0 \pm 2.2 \pm 1.1 \pm 1.1$
	Theory	$(93.5 \pm 20.5^a, 22.1 \pm 6.1^b)^{[2]}$ $11.9 \sim 15.1^{[3]}$	– $3.9^{[22]}$	$(15.2 \pm 1.7^a, 4.3 \pm 0.6^b)^{[2]}$ $3.5^{[22]}$
$\Sigma^0\bar{\Sigma}^0$	This work	$47.8 \pm 3.4 \pm 3.9$	$3.8 \pm 1.0 \pm 0.5 (< 6.2)$	$4.0 \pm 1.1 \pm 0.5 (< 6.5)$
	PDG	$42.0 \pm 7.0$	$< 4.0$	$< 8.0$
	CLEO	$44.1 \pm 5.6 \pm 4.2 \pm 2.2$	$< 4.4$	$< 7.5$
	Theory	$(25.1 \pm 3.4^a, 18.7 \pm 4.5^b)^{[2]}$ –	– $3.3^{[22]}$	$(38.9 \pm 8.8^a, 4.2 \pm 0.5^b)^{[2]}$ $5.0^{[22]}$
$\Sigma^+\bar{\Sigma}^-$	This work	$45.4 \pm 4.2 \pm 3.0$	$5.4 \pm 1.5 \pm 0.5 (< 8.7)$	$4.9 \pm 1.9 \pm 0.7 (< 8.8)$
	PDG	$31.0 \pm 7.0$	$< 6.0$	$< 7.0$
	CLEO	$32.5 \pm 5.7 \pm 4.0 \pm 1.7$	$< 6.5$	$< 6.7$
	Theory	$5.5 \sim 6.9^{[3]}$	$3.3^{[22]}$	$5.0^{[22]}$

238

239

## 240 VIII. SUMMARY

241 Three  $\chi_{cJ}$  decays to the baryon pairs are observed, and their branching fractions are mea-  
 242 sured at BESIII, which are consistent with the world averages within the errors. For the decay of  
 243  $\chi_{cJ} \rightarrow \Lambda\bar{\Lambda}$ , the experimental results are still inconsistent with theoretical predictions [2, 3, 22],  
 244 which are helpful to check the theoretical model of decays of  $\chi_{cJ} \rightarrow \Lambda\bar{\Lambda}$ . For the decays of  
 245  $\chi_{c1,2} \rightarrow \Sigma^0\bar{\Sigma}^0$  and  $\Sigma^+\bar{\Sigma}^-$ , the significances are improved relative to the previous measurments,  
 246 but the comparisons of their branching fractions between experiments and theoretical predictions  
 247 are inconclusive due to the limited experimental precision.

248 **IX. ACKNOWLEDGEMENT**

249 The BESIII collaboration thanks the staff of BEPCII and the computing center for their hard  
250 efforts. This work is supported in part by the Ministry of Science and Technology of China under  
251 Contract No. 2009CB825200, 2009CB825206; National Natural Science Foundation of China  
252 (NSFC) under Contracts Nos. 10625524, 10821063, 10825524, 10835001, 10935007, 10975143,  
253 10975047, 10979008, 11125525, 11275057; Joint Funds of the National Natural Science Foun-  
254 dation of China under Contracts Nos. 11079008, 11079027, 11179007; the Chinese Academy  
255 of Sciences (CAS) Large-Scale Scientific Facility Program; CAS under Contracts Nos. KJCX2-  
256 YW-N29, KJCX2-YW-N45; 100 Talents Program of CAS; Istituto Nazionale di Fisica Nucle-  
257 are, Italy; Ministry of Development of Turkey under Contract No. DPT2006K-120470; U. S.  
258 Department of Energy under Contracts Nos. DE-FG02-04ER41291, DE-FG02-91ER40682, DE-  
259 FG02-94ER40823; U.S. National Science Foundation; University of Groningen (RuG) and the  
260 Helmholtzzentrum fuer Schwerionenforschung GmbH (GSI), Darmstadt; WCU Program of Na-  
261 tional Research Foundation of Korea under Contract No. R32-2008-000-10155-0.

- 
- 262 [1] G. T. Bodwin, E. Braaten and G. P. Lepage, Phys. Rev. D **51**, 1125 (1995).  
263 [2] R. G. Ping, B. S. Zou and H. C. Chiang, Eur. Phys. J. A **23**, 129 (2004).  
264 [3] X. H. Liu and Q. Zhao, J. Phys. G **G38**, 035007 (2011).  
265 [4] K. Nakamura *et al.* (Particle Data Group), J. Phys. G **37**, 075021 (2012).  
266 [5] J. Z. Bai *et al.* (BES Collaboration), Phys. Rev. D **67**, 112001 (2003).  
267 [6] M. Ablikim *et al.* (BES Collaboration), Phys. Rev. D **73**, 052006 (2006).  
268 [7] P. Naik *et al.* (CLEO Collaboration), Phys. Rev. D **78**, 031101 (2008).  
269 [8] S. J. Brodsky and G. P. Lepage, Phys. Rev. D **24**, 2848 (1981).  
270 [9] M. Ablikim *et al.* (BESIII Collaboration), arXiv:1209.6199 [hep-ex].  
271 [10] M. Ablikim *et al.* (BESIII Collaboration), Nucl. Instrum. Meth. A **614**, 345 (2010).  
272 [11] S. Agostinelli *et al.* (GEANT4 Collaboration), Nucl. Instrum. Meth. A **506**, 250 (2003).  
273 [12] J. Allison *et al.*, IEEE Trans. Nucl. Sci. **53**, 270 (2006).  
274 [13] S. Jadach, B. F. L. Ward and Z. Was, Comput. Phys. Commun. **130**, 260 (2000),  
275 S. Jadach, B. F. L. Ward and Z. Was, Phys. Rev. D **63**, 113009 (2001).  
276 [14] R. G. Ping *et al.*, Chinese Physics C **32**, 599 (2008).  
277 [15] J. C. Chen, G. S. Huang, X. R. Qi, D. H. Zhang and Y. S. Zhu, Phys. Rev. D **62**, 034003 (2000).  
278 [16] Y. S. Zhu *et al.*, Chinese Physics C **32**, 363 (2008).  
279 [17] W. M. Tanenbaum *et al.*, Phys. Rev. D **17**, 1731 (1978),  
280 G. Karl, S. Meshkov and J. L. Rosner, Phys. Rev. D **13**, 1203 (1976),  
281 M. Oreglia *et al.*, Phys. Rev. D **25**, 2259 (1982).  
282 [18] M. Ablikim *et al.* (BESIII Collaboration), Phys. Rev. D **83**, 112005 (2011).  
283 [19] V. V. Anashin *et al.* (KEDR Collaboration), arXiv:1012.1694 [hep-ex].  
284 [20] R. E. Mitchell *et al.* (CLEO Collaboration), Phys. Rev. Lett. **102**, 011801 (2009).  
285 [21] G. R. Liao, R. G. Ping and Y. X. Yang, Chin. Phys. Lett. **26**, 051101 (2009).  
286 [22] S. M. H. Wong, Eur. Phys. J. C **14**, 643 (2000).